

An investigation of the role of radiative and non-radiative recombination processes in InAs/GaAs_{1-x}Sb_x quantum dot solar cells

Y. Cheng¹, A. J. Meleco¹, A. J. Roeth¹, V. R. Whiteside¹, M. C. Debnath¹, T. D. Mishima¹, M. B. Santos¹, S. Hatch², H-Y. Liu², and I. R. Sellers¹

¹HOMER L. DODGE DEPARTMENT OF PHYSICS & ASTRONOMY, UNIVERSITY OF OKLAHOMA, NORMAN, OK

²DEPARTMENT OF ELECTRICAL & ELECTRONIC ENGINEERING, UNIVERSITY COLLEGE LONDON, TORRINGTON PLACE. LONDON. WC1E 7JE. U. K

Abstract — An InAs/GaAs_{0.86}Sb_{0.14} QDSC and a GaAsSb control cell were investigated using temperature dependent J - V , external quantum efficiency (EQE), photoluminescence (PL) and electroluminescence (EL) measurements. Thermally activated defect states associated with the GaAsSb matrix materials are found to account for the reduction of the performance of the solar cell. The rapid quenching of the PL and EL intensity, along with the shift (above 150 K) of the dominant recombination process during spontaneous emission (EL) further indicate the prevalence of non-radiative processes at elevated temperatures in these systems. These findings are supported by a reduction in the open circuit voltage at elevated temperatures in these devices.

I. INTRODUCTION

Intermediate band solar cells (IBSC) [2] have been proposed as a candidate material system to go beyond the Shockley-Queisser limit [1]; i.e., the efficiency limit ($\sim 30\%$) of single band gap solar cells [1]. Through additional absorption of sub-band gap photons, a potential efficiency of $> 60\%$ has been predicted for IBSCs under ideal conditions [1][3]. The formation of the Intermediate band (IB) requires an isolated band situated within the band gap of the active region. Semiconductor quantum dots (QDs) are considered as a candidate system to form such IBs because of the discrete energy levels introduced by the 3-dimensional confinement of QDs. Several QD systems have been investigated over the past decade [4]-[9] where the most well-studied material system for IBSC applications is the InAs/GaAs QD system [4]-[6][9][11]. Despite significant progress, the practical potential of the InAs/GaAs QD system is limited by non-optimized spectral overlap and lower QD absorption [13]. By replacing the GaAs matrix material with GaAsSb, a higher density of QDs has been demonstrated [12][18]. This, coupled with a better spectral overlap of the InAs/GaAsSb system to the solar spectrum, make this system an interesting alternative for QD IBSCs [13].

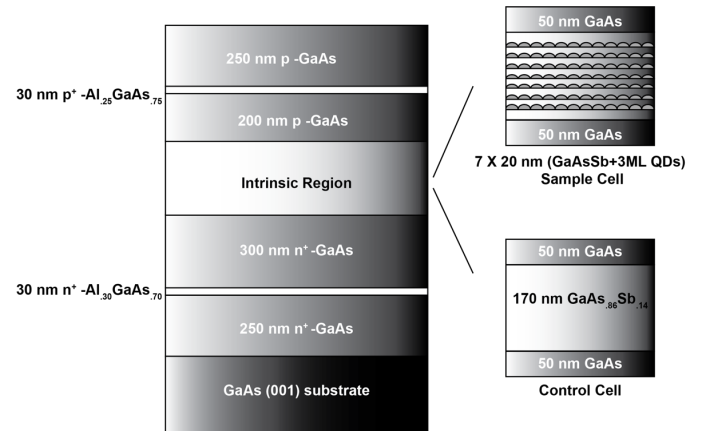


Figure 1 Schematic plot of the p-i-n GaAs solar cell structure: (a) Control cell, (b) InAs/GaAs_{0.86}Sb_{0.14} QDSC

II. EXPERIMENT DETAILS

A schematic of the comparative structures investigated in this manuscript is presented in Figure 1. Two p-i-n GaAs solar cells with different intrinsic materials were grown by molecular beam epitaxy (MBE). The basic structure consists of 250 nm of n-type GaAs ($1 \times 10^{18} \text{ cm}^{-3}$) grown on top of an GaAs (001) substrate. This is followed by a 30 nm n-Al_{0.30}GaAs_{0.70} ($5 \times 10^{17} \text{ cm}^{-3}$) back-surface field layer, and a 300 nm n-type GaAs ($2 \times 10^{17} \text{ cm}^{-3}$) buffer layer, which completes the base region of the solar cell. The intrinsic region for the QD containing structure consists of two 50 nm GaAs layers sandwiching 7 periods of InAs QDs in a GaAs_{0.86}Sb_{0.14} matrix. Each individual period (or QD layer) has a 20 nm GaAsSb layer upon which 3 monolayers (ML) of InAs is deposited to form the QDs. The final period of the QD stack is capped with a 30 nm GaAsSb layer; the total thickness of the intrinsic region is 270 nm (Figure 1). The intrinsic region of the control cell (a) has two 50 nm GaAs layers sandwiching 170 nm of GaAsSb. An Sb composition of 14% is chosen (based on a previous study for this material system[12, 18]) to achieve quasi-flat valence band (VB) conditions.

Temperature dependent (TD) current density-voltage (J - V) measurements were performed in a Linkam THMS600E micro cryostat with a Keithley 2400 multimeter and a Newport Oriel

Sol2A solar simulator. An Oriol Merlin digital lock-in radiometry system with an Oriol 300-watt xenon arc lamp and a quartz tungsten halogen (QTH) lamp was used to take the external quantum efficiency (EQE) measurements. Photoluminescence (PL) was carried out in a Janis cryostat with a HeNe laser excitation wavelength of 632.8 nm. A Princeton Instruments spectrometer fitted with a Roper Scientific liquid nitrogen (LN₂) cooled InGaAs linear array was used to collect the signal. Electroluminescence (EL) was taken with a Spex 270M spectrometer and Edinburgh Instruments LN₂-cooled Ge detector.

III. RESULTS AND DISCUSSIONS

Figure 2 shows the PL spectra of the (a) QD and (b) control cells from 4 K to 200 K. Peaks related to the GaAs-related transition(s) are seen in both the QD and control cells; displaying the Varshni [19] shift to longer wavelength as a function of increasing temperature (830 - 850 nm). A peak related to the InAs/GaAsSb QDs transition (from VB to IB) is observed in the QD cell (Figure 2 (a)); similarly, displaying a shift to longer wavelengths (1080 - 1120 nm) with increasing temperature. The peak intensity of the QD transition as a function of temperature is shown in the inset to Figure 2(a). The signal related to GaAsSb is not very pronounced in the QD structure as compared with the control cell (Figure 2 (b) 910 - 975 nm). The presence of a broad defect-related peak (950 - 1500 nm) is also evident in the control cell across the full temperature range investigated. In contrast, the defect peak becomes *more* evident in the QD cell above 150 K. This defect band is attributed to strain and therefore dislocations caused by the large lattice mismatch between GaAs and GaAsSb [12][15].

The QD PL peak shows an asymmetric shape with a high-energy shoulder due to the inhomogeneity of the QDs, which is more prevalent at low temperature (4 - 120 K). The origin of the bimodality evident in these QDs is attributed to a combination of QD strain relaxation, composition variations, QD size differences in the intrinsic region. As the intrinsic region becomes thicker, the tensile strain between the InAs and GaAsSb tends to relax [22], [23]; which results in larger and more uniform QDs, thus a lower energy PL.

At elevated temperatures (120 - 150 K), the extra thermal energy helps to redistribute the carriers among the different QDs to the lowest energy levels, where the PL spectra are dominated by the larger QDs; which narrows the linewidth, see Figure 2(a). As the temperature increases, the PL linewidth increases, while the PL intensity quenches rapidly (Figure 2a inset). This reduction in the PL FWHM is related to thermal redistribution and enhanced carrier escape processes at increasing temperatures. In addition, at elevated temperatures a broad peak related to defects becomes more evident for the QD-containing structure (Figure 2a). This defect band reflects the contribution of dislocations in the matrix region of the sample that form since the thickness of the intrinsic region exceeds that of the critical thickness for

strain relaxation in this system (estimated to be 10 nm based on theoretical calculation [20]).

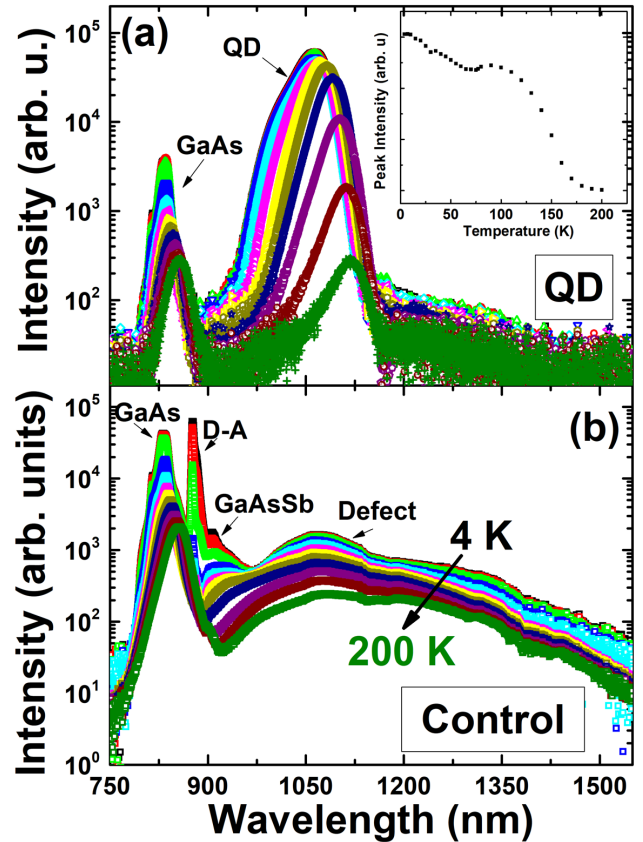


Figure 2 Temperature dependent PL measurement results of (a) the QD solar cell and (b) the control cell from 4 K to 200 K. Inset to (a) is the plot of PL peak intensity related to QDs as a function of temperature.

Figure 3 (a) and (b) compare the J - V measurements for the control and QD cells under illumination as a function of temperature. There are two main features evident in these data: a large reduction of the open circuit voltage (V_{oc}) and a noticeable influence of series resistance and inhomogeneity in the QD cell (Figure 3b).

At low temperatures (77 - 150 K), the influence of series resistance and the multimodal behavior (0.8 - 1.0 V inset of Figure 3 (a)) is evident in the QD cell. This is consistent with PL measurements (see Figure 2a), where the photo-generated carriers are isolated in QDs of different sizes at lower temperatures and therefore result in strong luminescence from the individual subsets of QDs. The effect in the J - V measurements is a higher series resistance, due to inhibited carrier transport, and noticeable inflections in the light J - V measurements below $T = 150$ K. Although not dominant, localization in defects at lower temperatures also contributes to the resistance, which can be seen at low temperatures for the control structure in Figure 3(b). As the temperature is increased, there is a notable, and dramatic, reduction of V_{oc} observed for both cells; such a massive reduction of V_{oc} is

related to defect induced non-radiative recombination. The increasing recombination current contributes to the dark saturation current and decreases the V_{oc} significantly. The large effect of dark current losses is directly related to defect states and dislocations associated with the lattice mismatch between GaAs and GaAsSb.

The TD J - V measurements are summarized in Figure 4. Figure 4(a) compares V_{oc} of the control cell (solid black circles) and the QDSC (solid red triangles). At 77 K, an V_{oc} of 1.18 V under 1 sun illumination is observed for the control cell. The V_{oc} measured for the QD cell is ~ 1.1 V, slightly smaller than the control cell, which is expected due to the additional recombination path provided by the QDs in the active region [21]. Moreover, the larger differential V_{oc} provided by the QDs (~ 0.08 V) at lower temperature is associated with a greater series resistance caused by the localization of carriers in dots, as compared with the V_{oc} reduction (~ 0.03 V) above 150 K.

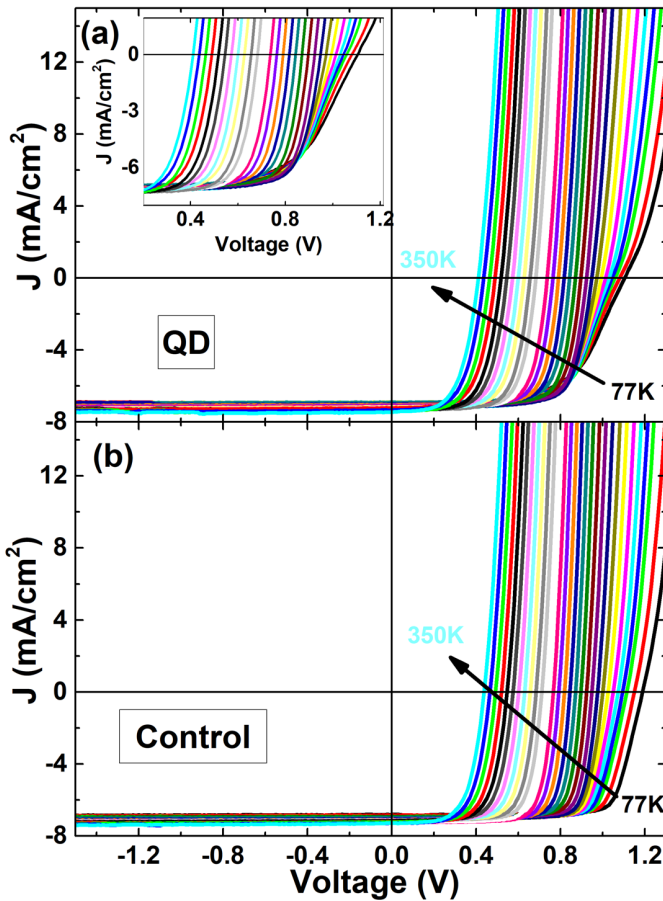


Figure 3 Temperature dependent J - V measurements for the (a) QD cell and (b) control cell under illumination. Inset to (a) is a zoom in of light J - V of QD cell.

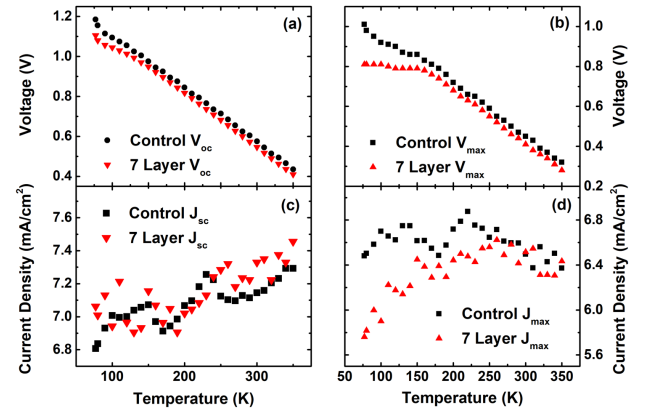


Figure 4 Temperature dependent (a) V_{oc} , (b) V_{max} , (c) J_{sc} , and (d) J_{max} for control (black squares) and QD cells (red triangles).

Figure 4(b) and (d) compare V_{max} and J_{max} , respectively, for the control and QD SCs. These maximum current density and voltage points represent the values determined from the maximum power point of the illuminated J - V responses as a function of temperature. For the QD cell (closed red triangles), as the temperature increases from 77 K to 150 K, V_{max} is relatively stable despite V_{oc} dropping considerably. This difference in the behavior of the maximum and open circuit voltages with increasing temperature reflects the improvement in the fill factor as the series resistance is reduced at elevated temperatures, as carriers escape for the QDs and localized centers in the matrix. This behavior is also clearly reflected in the increasing J_{max} over this temperature range. Above 150 K, the escape from the QDs supercedes the confinement of QDs, and V_{max} now follows the steady decreasing trend of the V_{oc} . These data indicate that at $T < 150$ K, where photogenerated carriers are localized in the QDs, the properties of the QDSC are mainly determined by carrier transport to and from the QDs. Above 150 K as carriers redistribute and escape the dots, defects in the matrix control the system response. This is evident in the consistency of J_{sc} , J_{max} , V_{oc} , and V_{max} in Figure 4 above 150 K. This is also strongly related to the quenching of the PL at $T > 150$ K (see Figure 2a) where carrier escape quenches the luminescence intensity considerably.

On the other hand, the carriers in the control cell are relatively delocalized; thus these carriers interact with non-radiative centers (defect states) more readily, and the maximum power point decreases monotonically as more defect states become activated with the increasing temperature. The increased contribution of non-radiative centers at elevated temperatures is likely due to the ionization of localized impurities on these centers that reveal deleterious trap states at higher temperatures [24]. The competing process of thermally activated non-radiative recombination and thermal escape of carriers from the QDs results in a complex J_{sc} behavior as illustrated by the non-monotonic behavior of J_{sc} in Figure 4(c). The J_{sc} fluctuates until the temperature goes above 240 K, where the thermal escape becomes a more

efficient process than the non-radiative recombination, and the J_* keeps increasing.

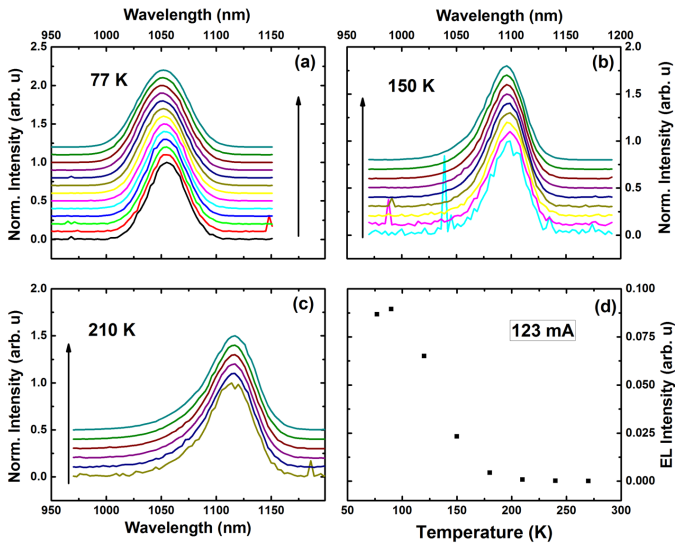


Figure 5 *EL* spectra for the QD cell as a function of injection current at temperatures of (a) 77 K, (b) 150 K, and (c) 210 K. (d) *EL* intensity at 123 mA injection current as a function of temperature.

In addition to *PL* measurements, electroluminescence (*EL*) measurements were carried out on the cells. However, no *EL* signal is seen from 800 nm to 1700 nm for the control cell; the lack of an *EL* signal is attributed to a combination of limited carrier localization in the intrinsic region, and efficient non-radiative processes in the control cell. Figure 5 shows *EL* spectra at different current injection levels at four temperatures for the QD cell. At 77 K, a blue shift is observed as the current injection increases. As noted in the *PL* measurements, the InAs/GaAsSb QDs are not uniform, and therefore exhibit the effects of inhomogeneity such as carrier redistribution and competing QD ensembles at lower temperatures as is evident in Figure 5(a). At higher temperatures (150 K and above), the additional thermal energy redistributes the carriers, allowing them to recombine in the lowest energy states. Thus, the peak position remains relatively constant at the elevated injection level as is evident in Figures 5(b) and (c), which show the *EL* at 150 K and 210 K, respectively. The peak intensity at a 123 mA injection level as a function of temperature is summarized in Figure 5 (d). The peak intensity remains relative constant below 120 K; while quenching rapidly above 120 K. This behavior reflects that of the TD *PL* measurements (Figure 2 (a) inset) providing further evidence for carrier escape at elevated temperatures.

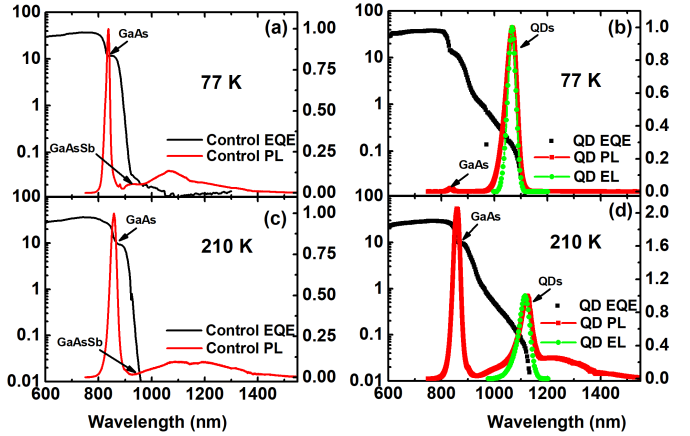


Figure 6 *PL* (red) and *EQE* (black) measurements for the control cell at (a) 77 K and (c) 210 K. *EQE* (black), *PL* (red), and *EL* (green) measurements for the 7 Layer QD cell at (b) 77 K and (d) 210 K.

Figure 6 compares the *PL*, *EL*, and *EQE* at 77 K (a, b) and 210 K (c, d) for both the control (a, c) and QD cells (b, d). The *EQE* and *PL* of the control cell indicate that the photo-generated carriers are indeed related to the GaAs and GaAsSb transitions; defect states are also observed in *PL* measurements. As mentioned before, the intrinsic region of the control cell is GaAsSb, which without employing any strain balancing techniques contains many defects; these defects serve as non-radiative recombination centers. As the temperature increases, the signal from GaAsSb quenches quickly; thermal broadening of both the GaAs peak and the defect band is also noted.

A comparison of the *EQE*, *PL*, and *EL* of the QD cell at 77 K (b) and 210 K (d) indicates that the additional increase of the photocurrent as seen in the *EQE* comes from the QD transition (above 950 nm); i.e., the VB to IB transition in the active region of the device. At 77 K, there are two extra features in the *PL* measurements not seen in the *EL*: at ~840 nm and ~910 nm (not very pronounced); which correlate to the transitions for the GaAs and GaAsSb matrix, respectively. The absence of these features in the *EL* measurements across the whole temperature range reflects the direct injection of the carriers into the QDs and the separation of the quasi-Fermi level that is set by the difference in energy of the QD transitions in *EL*. In the *PL* measurements, the GaAs emitter and QDs are probed simultaneously [14], which with the combination of the longer radiative lifetime of photogenerated carriers in the type-II QDs, contributes to significant *PL* from the continuum regions.

At 210 K, the *PL* spectrum is normalized to the QD peak. The peak intensity of the QDs has a three order of magnitude reduction and a considerable contribution of the low energy defect states to the *PL*. As the temperature is increased above 210 K (not shown), the defect band transition dominates the *PL*. The peak intensity of the *EL* sees only one order of

reduction by 210 K, because of the direct injection of the carriers into the active region.

The carrier recombination processes are divided into two regimes: (1) a low temperature regime, where the radiative recombination within the QDs is more efficient, and the “frozen” defect states are not activated; (2) a higher temperature (> 150 K) region, where the additional thermal energy facilitates the carrier escape from the QDs, quenching the radiative recombination. This allows the Shockley-Read-Hall (SRH) recombination to dominate the recombination process at higher temperature (see Figure 7). At $T < 120$ K, the photo-generated carriers are localized in the QDs, the carriers are isolated from the SRH recombination centers; at higher temperatures, thermally activated carriers are captured by the activated SRH recombination centers, which quenches both the *PL* and *EL* signals.

This hypothesis that there is a thermally mediated transition from radiative to non-radiative processes in the *PL* and *EL* measurements above ~ 125 K is consistent with our unconventional TD *J-V* measurement results, where the V_c decreases significantly without a noticeable enhancement of J_c . The competition between the non-radiative recombination and thermal escape at high temperature therefore leads to the complex behavior of the *J-V* measurements as shown in Figure 3.

To further investigate these hypotheses, here, the spontaneous emission in *EL* measurements is analyzed to determine the nature and dominance of the recombination processes under different conditions and correlate these findings to the PV analysis. The current injected into a device can be approximated by [16]:

$$I = eV(An + Bn^2 + Cn^3) + I_{leak} . \quad (1)$$

Where A , B , and C represent: single carrier recombination, radiative recombination, and Auger process coefficients, respectively [16]. Here, V is the active region volume. Single carrier recombination is associated with the non-radiative processes recombination via traps and defects (SRH) [16]; the radiative recombination is related to the spontaneous emission (*EL*). The total integrated spontaneous emission rate L is proportional to the radiative recombination n^2 . Thus, the carrier concentration n is directly proportional to $L^{1/2}$. Then equation (1) is simplified to $I \propto n^z \propto L^{z/2}$ [16]. When radiative recombination dominates the current, the z -factor will be close to 2 ($\propto n^2$). However, if z is close to 1 ($\propto n$), this indicates the current is dominated by non-radiative recombination centers - defects and traps. By plotting $\ln(I) - \ln(L^{1/2})$, the z -factor is extracted directly from the slope of the response to determine the nature of the dominant recombination processes.

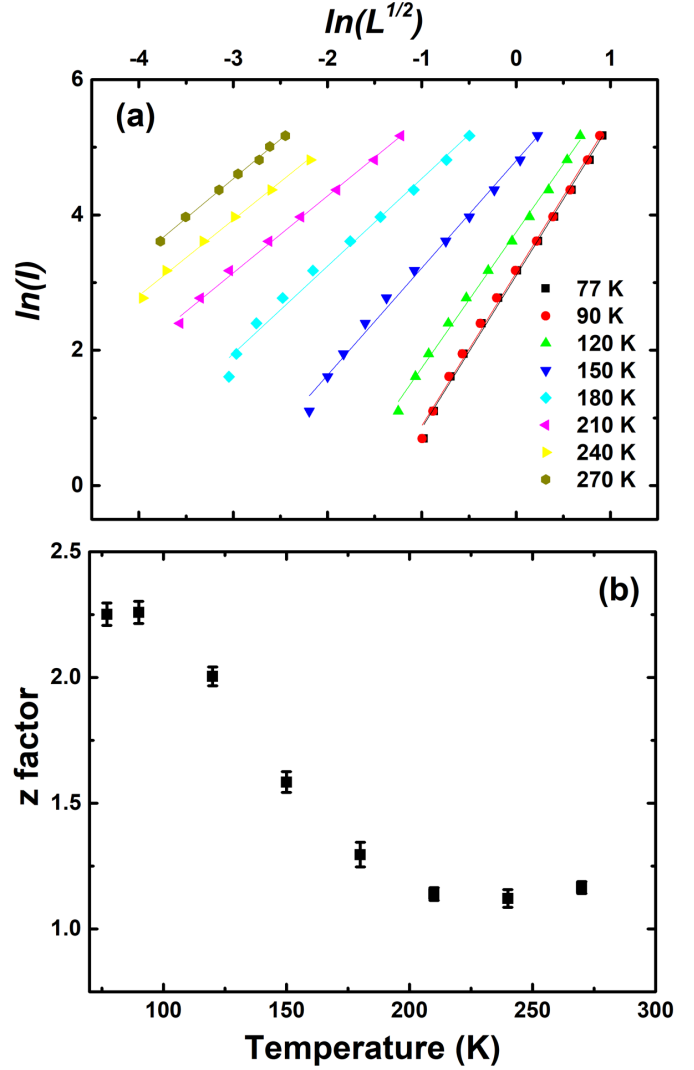


Figure 7 (a) $\ln(I) - \ln(L^{1/2})$ plot from 77 K to 270 K; (b) Temperature dependent behavior of z factor.

The $\ln(I) - \ln(L^{1/2})$ plots for the QDSCs at various temperatures are shown in Figure 7 (a), where different gradients are clearly evident with increasing temperature: a steeper the slope reflects a larger the z -factor. The temperature dependence of the z -factor for the QDSC is summarized in Figure 7 (b). The difference of the slopes suggests different mechanisms dominate the recombination process in different temperature regimes. At $T < 120$ K, z -factors of around 2 are observed, which indicates that the dominant recombination process is radiative. Although a $z = 3$ reflects non-radiative Auger processes, which may be invoked at $T < 100$ K in Figure 7(b), such processes are not considered significant here. Auger processes are usually problematic at high injection currents, which were not necessary due to the strong luminescence efficiency. Here, the value of $z > 2$ at $T < 100$ K is rather attributed to inhomogeneities in the QD

distribution and the contribution to subsets of QDs to the *EL* at lower temperatures.

At $T > 125$ K (150 K and above) a rapid reduction of the *z*-factor towards $z = 1$ is evident. Such behavior indicates that SRH (non-radiative) recombination becomes dominant, which directly corresponds to the temperature dependent quenching of the *EL* and *PL* intensity and the massive reduction of the V_c at $T > 150$ K. This further supports the hypothesis that thermally activated carriers that escape from the QDs are trapped in defect states and on non-radiative channels in the matrix and thus not collected effectively, following the limited performance of the control cell. At higher temperature, higher injection currents are required to produce reasonable *EL*. This behavior provides further evidence for the important role of non-intentional impurities that are localized on traps at lower temperatures, which increased the concentration of available non-radiative centers at higher temperature.

IV. CONCLUSION

An InAs/GaAs_{0.98}Sb_{0.02} QD cell and a GaAsSb control cell were investigated using complementary *PL* and *EL* measurements. Defect states associated with the lattice mismatch between GaAsSb and GaAs are proposed to account for the limited performance of the solar cell. A rapid quenching of the *PL* and *EL* intensity, along with a simultaneous decrease in the *z*-factor from 2 to 1 (above 150 K) in the *EL* analysis, indicating a transition from radiative to non-radiative dominated recombination, further demonstrates the prevalence of non-radiative processes at elevated temperatures in these systems. This correlates qualitatively with TD *EQE* and *J-V* measurements - supporting the conclusion that the loss of carriers comes from the thermally activated defect states in the GaAsSb matrix at higher temperatures.

V. ACKNOWLEDGMENT

The authors acknowledge financial support through the NASA EPSCoR program, Grant(s) #NNX15AM75A, and #NNX13AN01A. Support is also acknowledged from the state of Oklahoma OCAST program, Grant No. # AR12.2-043.

REFERENCES

[1] W. Shockley and H. J. Queisser, "Detailed balance limit of efficiency of p - n junction solar cells." *Journal of applied physics* 32.3 (1961): 510-519.
 [2] A. Luque, and A. Martí. "Increasing the efficiency of ideal solar cells by photon induced transitions at intermediate levels." *Physical Review Letters* 78.26 (1997): 5014.
 [3] A. Luque and A. Martí, "The intermediate band solar cell: progress toward the realization of an attractive concept." *Advanced Materials* 22, no. 2 (2010): 160-174.
 [4] S. M. Hubbard, C. D. Cress, C. G. Bailey, R. P. Raffaele, S. G. Bailey, and D. M. Wilt, "Effect of strain compensation on quantum

dot enhanced GaAs solar cells." *Applied Physics Letters* 92, no. 12 (2008): 123512.
 [5] G. Jolley, H. F. Lu, L. Fu, H. H. Tan, and C. Jagadish, "Electron-hole recombination properties of In_{0.5}Ga_{0.5}As/GaAs quantum dot solar cells and the influence on the open circuit voltage." *Applied Physics Letters* 97, no. 12 (2010): 123505.
 [6] K. A. Sablon, J. W. Little, K. A. Olver, Z. M. Wang, V. G. Dorogan, Y. I. Mazur, G. J. Salamo, and F. J. Towner, "Effects of AlGaAs energy barriers on InAs/GaAs quantum dot solar cells." *Journal of Applied Physics* 108, no. 7 (2010): 074305.
 [7] P. J. Simmonds, R. B. Laghumavarapu, M. Sun, A. Lin, C. J. Reyner, B. Liang, and D. L. Huffaker, "Structural and optical properties of InAs/AlAsSb quantum dots with GaAs (Sb) cladding layers." *Applied Physics Letters* 100, no. 24 (2012): 243108.
 [8] R. B. Laghumavarapu, A. Moscho, A. Khoshakhlagh, M. El-Emawy, L. F. Lester, and D. L. Huffaker, "GaSb / GaAs type II quantum dot solar cells for enhanced infrared spectral response." *Applied Physics Letters* 90, no. 17 (2007): 173125.
 [9] S. Hatch, J. Wu, K. Sablon, P. Lam, M. Tang, Q. Jiang, and H. Liu, "InAs/GaAsSb quantum dot solar cells." *Optics express* 22, no. 103 (2014): A679-A685.
 [10] F. K. Tutu, I. R. Sellers, M. G. Peinado, C. E. Pastore, S. M. Willis, A. R. Watt, T. Wang, and H. Y. Liu, "Improved performance of multilayer InAs/GaAs quantum-dot solar cells using a high-growth-temperature GaAs spacer layer." *Journal of Applied Physics* 111, no. 4 (2012): 046101.
 [11] A. Martí, E. Antolín, C. R. Stanley, C. D. Farmer, N. López, P. Díaz, E. Cánovas, P. G. Linares, and A. Luque. "Production of photocurrent due to intermediate-to-conduction-band transitions: a demonstration of a key operating principle of the intermediate-band solar cell." *Physical Review Letters* 97, no. 24 (2006): 247701.
 [12] Y. Cheng, M. Fukuda, V. Whiteside, M. Debnath, P. Valley, T. Mishima, M. Santos, K. Hossain, S. Hatch, H. Liu, and I. R. Sellers. "Investigation of InAs/GaAs_{0.98}Sb_{0.02} quantum dots for applications in intermediate band solar cells." *Solar Energy Materials and Solar Cells* 147 (2016): 94-100.
 [13] M. Y. Levy and C. Honsberg, "Nanostructured absorbers for multiple transition solar cells." *IEEE Transactions on Electron Devices* 55, no. 3 (2008): 706-711.
 [14] I. Ramiro, E. Antolín, P. G. Linares, E. Hernández, A. Martí, A. Luque, C. Farmer, and C. Stanley. "Application of photoluminescence and electroluminescence techniques to the characterization of intermediate band solar cells." *Energy Procedia* 10 (2011): 117-121.
 [15] Y. Cheng, M. Fukuda, V. R. Whiteside, M. C. Debnath, P. J. Valley, A. J. Meleco, A. J. Roeth et al. "Investigation of InAs/GaAs_{0.98}Sb_{0.02} quantum dots for applications in intermediate band solar cells." *Photovoltaic Specialists Conference (PVSC)*, 2016 IEEE 43rd, pp. 0005-0008, 2016
 [16] A. F. Phillips, S. J. Sweeney, A. R. Adams, and P. J. Thijs. "The temperature dependence of 1.3- and 1.5- μ m compressively strained InGaAs (P) MQW semiconductor lasers." *IEEE Journal of selected topics in quantum electronics* 5, no. 3 (1999): 401-412.
 [17] B. Williams, S. Smit, B. Kniknie, K. Bakker, W. Keuning, W. Kessels, R. Schropp and M. Creatore, "Identifying parasitic current pathways in CIGS solar cells by modeling dark J-V response." *Progress in Photovoltaics: Research and Applications* 23, no. 11 (2015): 1516-1525.
 [18] M. C. Debnath, T. D. Mishima, M. B. Santos, Y. Cheng, V. R. Whiteside, I. R. Sellers, K. Hossain, R. B. Laghumavarapu, B. L. Liang, and D. L. Huffaker. "High-density InAs/GaAs_{1-x}Sb_x quantum-dot structures grown by molecular beam epitaxy for use in

- intermediate band solar cells." *Journal of Applied Physics* 119, no. 11 (2016): 114301.
- [19] Varshni, Yatendra Pal. "Temperature dependence of the energy gap in semiconductors." *Physica* 34, no. 1 (1967): 149-154.
- [20] Matthews, J. W. "Defects associated with the accommodation of misfit between crystals." *Journal of Vacuum Science and Technology* 12, no. 1 (1975): 126-133.
- [21] Martí, A., E. Antolín, E. Cánovas, N. López, P. G. Linares, A. Luque, C. R. Stanley, and C. D. Farmer. "Elements of the design and analysis of quantum-dot intermediate band solar cells." *Thin solid films* 516, no. 20 (2008): 6716-6722.
- [22] Kim, Yeongho, Keun-Yong Ban, Chaomin Zhang, Jun Oh Kim, Sang Jun Lee, and Christiana B. Honsberg. "Efficiency enhancement in InAs/GaAsSb quantum dot solar cells with GaP strain compensation layer." *Applied Physics Letters* 108, no. 10 (2016): 103104.
- [23] Liu, H. Y., I. R. Sellers, R. J. Airey, M. J. Steer, P. A. Houston, D. J. Mowbray, J. Cockburn, M. S. Skolnick, B. Xu, and Z. G. Wang. "Room-temperature, ground-state lasing for red-emitting vertically aligned InAlAs/AlGaAs quantum dots grown on a GaAs (100) substrate." *Applied physics letters* 80, no. 20 (2002): 3769-3771.
- [24] Brown, C. R., N. J. Estes, V. R. Whiteside, B. Wang, K. Hossain, T. D. Golding, M. Leroux et al. "The effect and nature of N-H complexes in the control of the dominant photoluminescence transitions in UV-hydrogenated GaInNAs." *RSC Advances* 7, no. 41 (2017): 25353-25361.